A 700 MHz laser radar receiver realized in 0.18 µm HV-CMOS

Mikko Hintikka; Juha Kostamovaara

Department of Information and Electrical Engineering, Circuits and Systems Research Group, University of Oulu, Linnanmaa, Finland

This is a post-peer-review, pre-copyedit version of an article published in Analog Integr Circ Sig Process.

The final authenticated version is available online at: http://dx.doi.org/10.1007/s10470-017-1041-0.

ABSTRACT

This study presents a CMOS receiver chip realized in 0.18 µm High-Voltage CMOS (HV-CMOS) technology and intended for high precision pulsed time-of-flight laser range finding utilizing high-energy sub-ns laser pulses. The IC chip includes a trans-impedance preamplifier, a post-amplifier and a timing comparator. Timing discrimination is based on leading edge detection and the trailing edge is also discriminated for measuring the width of the pulse. The transimpedance of the channel is 25 kΩ, the uncompensated walk error is 470 ps in the dynamic range of 1:21,000 and the input referred equivalent noise current 450 nA (rms).

Keywords:- laser radar receiver; laser ranging; optical sensors; timing discrimination

1 INTRODUCTION

The pulsed time-of-flight laser range finding principle is based on the measurement of a transit time of a short laser pulse travelling from the laser transmitter to the target and back to the pulse detector electronics. The measured flight time of the pulse can be converted to a distance of the target based on the known velocity of light. Fig. 1 shows a typical construction of a pulsed TOF laser range finder. The achievable precision is typically at the level centimeters. [1]

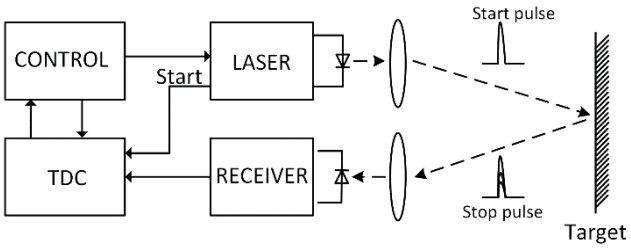

Fig. 1 Block diagram of a TOF based laser radar

Since the use of optical signals for measuring distances removes the need for physical contact with the target, laser range finding has been applied in many fields, including the automotive, military or robotics for target identification and range determination [2–4]. The unique advantages of the pulsed TOF range finding technique, are high precision and short measurement time. It also gives a high spatial resolution due to the fact that electromagnetic radiation at optical frequencies can easily be focused with optical lenses.

The main factors limiting the measurement accuracy of a TOF laser radar are noise limiting the single shot-precision and amplitude variation of the received echo causing systematic timing error (known as timing walk). Typical TOF based laser radars are using laser pulses with a pulse width of 3 – 5 ns limited by the limitations of high-speed laser diode drivers [5]. However, in principle, the single-shot accuracy, timing walk as well as eye-safety could be improved if shorter, even sub-ns pulses, were used. This would also help detecting multiple targets within the measurement range. Recently, techniques to produce high-energy sub-ns pulses with semiconductor laser diodes have been presented, and thus there is an interest to study what kind of performance would be available in laser ranging using these transmitter techniques [6–9].

In this work, a laser radar receiver that can be used to detect high-energy sub-ns pulses has been designsed and chracterized. The proposed integrated CMOS laser radar receiver is designed for a fast and accurate pulsed TOF laser range finder especially targeted to measure small distance variations of a distant target e.g. for measuring the vibration of a surface at some distance.

The paper is organized as follows. Section II describes the sub-ns pulse detection from the accuracy and precision points of view. The construction and an implementation of the receiver channel are presented in section III. Section IV presents the most essential verification results from the chip. Conclusions are given in section V.

2 SUB-NS LASER PULSE DETECTION

Typical pulsed TOF laser range finders nowadays use 3 – 5 ns laser pulse in the transmitter. Even though the usage of a shorter pulse width would be beneficial from the accuracy point of view, the problem is that the peak power level available from commercial laser diode sources giving a single sub-ns pulse is limited to sub-W range [10, 11]. However, recently, a number of special gain-switched laser constructions have been suggested to increase the available energy level [6, 9, 12, 13]. A particularly interesting semiconductor laser approach is based on the "enhanced gain switching" principle, which is capable of producing laser pulses with an energy level and pulse width of ~ 1 nJ and ~ 100 ps, respectively [7, 9]. A notable feature of this technology is that the driver requirements are quite moderate and can be straightforwardly realized with standard MOS circuit technology. The pulse transmitter used in the receiver verification measurements of this work is based on a MOSFET based driver presented in [8]. The transmitter utilizes a custom designed bulk laser diode working in the "enhanced gain switching" mode and it generates a 100 ps (FWHM) pulse with a peak power of 10 W at a wavelength of 860 nm. The properties of the sub-ns pulse detection are analyzed in the following subsections to motivate the receiver design.

2.2 Timing walk error

The amplitude of the received pulse in a pulsed TOF may vary a lot due to changes in the reflectivity, orientation and distance of the target. When using the leading edge timing discrimination principle, where the timing comparator generates the timing signal as the received echo pulse crosses a certain threshold at the input of the comparator, the amplitude variation causes timing error (typically known as timing walk error) [14]. The amount of walk error depends largely on the slew rate of the pulse. The shorter pulse rise time gives a lower walk error, as shown in Fig. 2 where three pulses with different pulse widths and rise times are shown with the corresponding timing walk error.

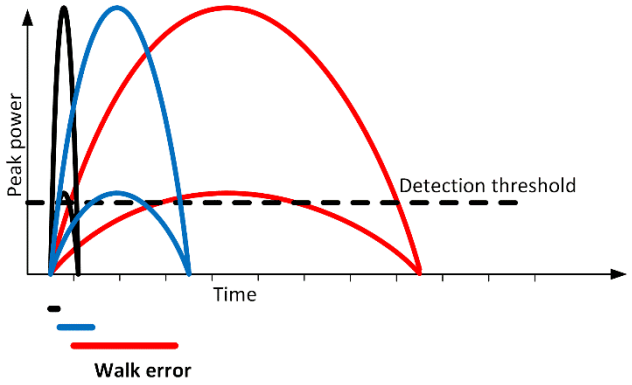

Fig. 2 Walk error

2.3 Noise and jitter

The input referred noise current is one of the most critical parameters in a trans-impedance amplifier (TIA), which is normally used as the preamplifier in a pulsed mode laser radar receiver. The noise of the TIA usually dominates over all the other noise sources in the amplifier channel and therefore determines the sensitivity of the receiver [15–19]. Fig 3 illustrates the definition of TIA noise as the equivalent input noise current $I_{n,\,TIA}$ at the input of the noiseless TIA. The equivalent input noise current source together with the noiseless TIA reproduces the output noise of the actual noisy TIA.

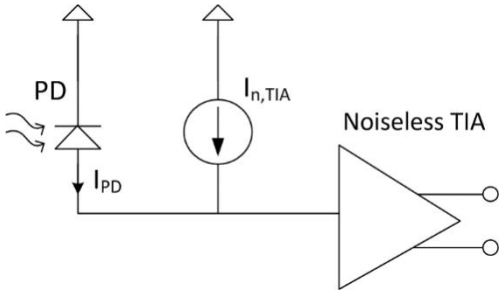

Fig. 3 TIA definition

The input referred RMS noise current relates directly the sensitivity of the laser radar receiver and can be expressed with a single number. It is determined by dividing the total RMS output noise voltage by the TIA's mid-band transimpedance value [15].

$$i_{n,rms} = \frac{1}{R_T}\sqrt{\int_0^{>2BW} |Z_T(f)|^2 \times I_n^2(f)df}\ , \qquad (1)$$

where $|Z_T(f)|$ is the frequency response of the transimpedance amplifier and R_T is its mid-band value.

The bandwidth of the TIA must be optimized so as to reduce the total integral noise. However, the bandwidth needs to be sufficient for detecting the pulses. The time bandwidth product optimizing the SNR for Gaussian shape pulses is defined to be 0.44, which means that the optical bandwidth is $0.44/T_P$ -, where T_P is the pulse width (FWHM) [20]. When increasing the bandwidth of the TIA while decreasing the pulse width, the noise is increasing under square root as in (1). That means that if the pulse width decreases by the factor of ten, for example, and thus the bandwidth of the TIA increases by the factor of ten correspondingly, the total noise increases roughly by a factor of three only. If the laser pulse energy can be kept constant, that will improve the signal-to-noise ratio and also the timing walk error. Fig. 4 shows three pulses with the same pulse energy but different pulse widths and the corresponding noise levels of the receiver. In reality this tendency is softer however since the spectral noise of the preamplifier also tends to become lower at lower bandwidths. [15]

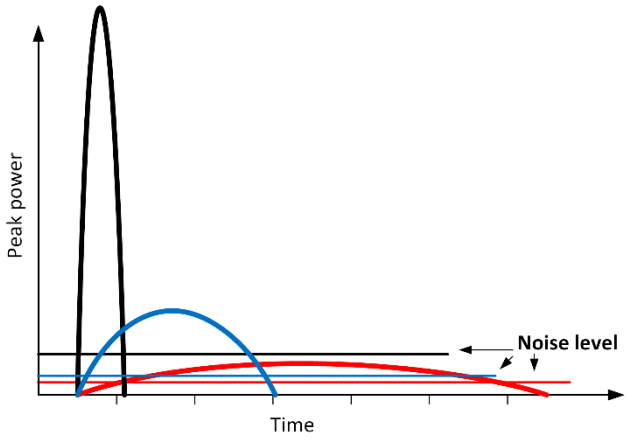

Fig. 4 Noise level vs. pulse width

The jitter in the pulse detection is proportional to the ratio of the receiver noise and the slew rate of the timing signal.

$$s_{jitter} \approx \frac{s_{noise}}{(\partial v/\partial t)} \approx \frac{t_r}{SNR} \qquad (2)$$

As already explained above, a shorter pulse with a certain energy improves the SNR and also has a shorter rise time, and thus the jitter in the detection is improved as well. [21] The above brief analysis shows thus that from the point of view of measurement accuracy it is in principle advantageous to shorten the laser pulse in laser ranging, especially if this can be done without decreasing the total energy of the pulse.

3 RECEIVER CHANNEL

Typically the receiver channel electronics used in a TOF based laser range finder consists of a trans-impedance pre-amplifier, a voltage type-post amplifier and a timing discrimination generating the timing mark from the received echo pulse. The distance measurement is based on the measurement of time interval between the generation of the laser pulse and the detection of the laser echo with the receiver. The bandwidth requirement for the receiver arises from the characteristics of the laser pulse used in the ranging. The receiver realized in this work includes the amplifier chain as mentioned above and also two timing comparators, which are used to detect the leading and the trailing edges of the analogue timing pulse at the output of the receiver channel. Both edges are discriminated for measuring the width of the received pulse. This information can be used for walk error compensation, for example. The optical pulse is converted to a current pulse in an external Avalanche Photo Detector (APD). Fig. 5 shows a simplified block diagram of the receiver chip realized in this work.

An APD with the diameter of 100 µm and internal capacitance of 0.5 pF was used as the photo detector of the receiver channel. The diameter selection is determined by the stripe width of the laser diode, since they should match [22]. Further minimizing the input capacitance the input pads with smallest ESD clamp diodes were used and unnecessary metal was removed from the pads. In [23] it was shown that the discrete high-speed APD outputs a ~ 300 ps pulse if a ~ 100 ps optical input pulse was used. As pointed out above, the bandwidth requirement for the channel becomes from the pulse width and ~ 300 ps means that the bandwidth of the receiver channel should be in the range of ~ 1 GHz. The maximum input signal from the APD can be however very high and thus the input current for the receiver channel was limited with external cross-coupled Schottky diodes. The transimpedance of the channel needs to be high enough to receive a small signal (slightly above the noise level) at the level detectable by the comparators. The input-referred noise current was estimated to be ~ 450 nA and thus the transimpedance of 25 kΩ gives ~ 11 mV noise voltage to the output of the channel. With this trans-impedance the signal level with a SNR of 10 is ~ 110 mV.

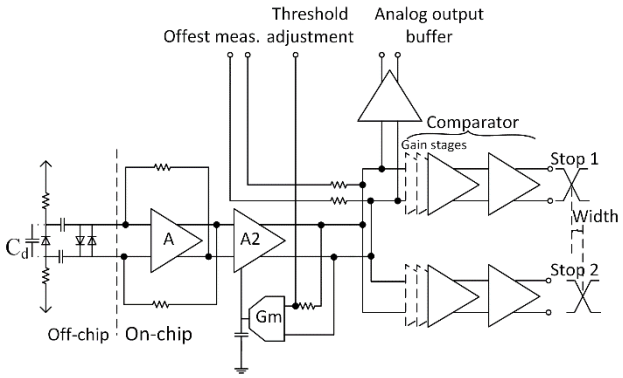

Fig. 5 Block diagram of the receiver

3.1 Receiver Stages

3.1.1 Preamplifier

The transimpedance preamplifier which is used to convert the APD current to a voltage signal includes the core amplifier with the active nested feedback topology and the overall shunt feedback resistors. Fig. 6 illustrates the topology as a single-ended version. The inner feedback loop makes a voltage amplifier compose of two transconductance gain stages (g_{m2}) and the active feedback (g_{mf}). Basically the inner amplifier follows the Cherry-Hooper topology, [24] yet with an active feedback. The outer loop with the passive shunt feedback resistor performs the current to voltage conversion. Basically three gain stages could

be used without the inner g_{mf} feedback loop but wide bandwidth requirement easily leads to stability problems due to the high gain. The use of g_{mf} improves the stability and thus the bandwidth as well. [25, 26]

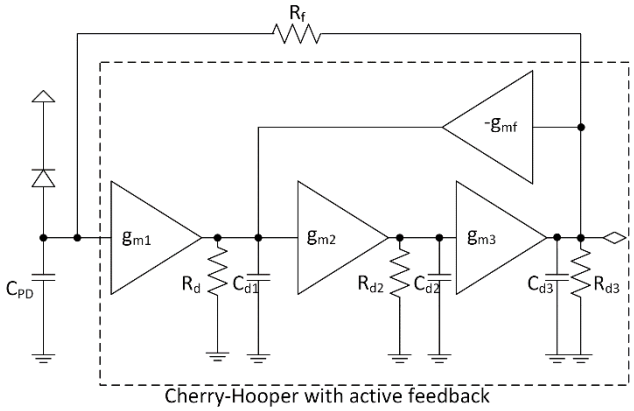

Fig. 6 Nested feedback structure

As already mentioned, the noise of the TIA is an important parameter which determines the sensitivity of the receiver and thus needs to be optimized. The first stage of the amplifier is dominating as a noise source and thus the noise model of the shunt feedback TIA can be simplified as in Fig. 7, where $I_{n,G}$ is small and can be neglected [15]. The input referred noise current $I_{n,TIA}^2$ can be derived as [15, 27]

$$I_{n,TIA}^2(f) = \frac{4kT}{R_f} + 4kT\Gamma \cdot \frac{1}{g_{m1}R_f^2} + 4kT\Gamma \cdot \frac{(2\pi C_T)}{g_{m1}} \cdot f^2, \qquad (3)$$

where Γ is the channel noise factor of the MOSFET and C_T is the total capacitance (capacitance of the photo diode C_{PD} and the input capacitance of the amplifier C_{IN}). It is seen that R_f and g_{m1} need to be as large as possible but any increase in g_{m1} will increase the input capacitance as well. As discussed in [28], there is an optimum value for input capacitance which should be matched with the external capacitance. So the W/L of the transistors in the input stage of the TIA were chosen to be 2,240 giving 0.34 pF gate capacitance for the input transistor. It is not as large as the C_{PD} (~ 1.5 pF with layout parasitics) but as is shown in [29] the noise optimum is broad and therefore the selected input transistor widths give a compromise between the noise and layout area . The lengths of the transistors at first stage were chosen to be 250 µm instead of the lowest allowed 180 µm to increase the r_{ds} of the transistors. The R_f was chosen to be 1.3 kΩ. Fig. 8 shows the detailed schematic of the differential TIA.

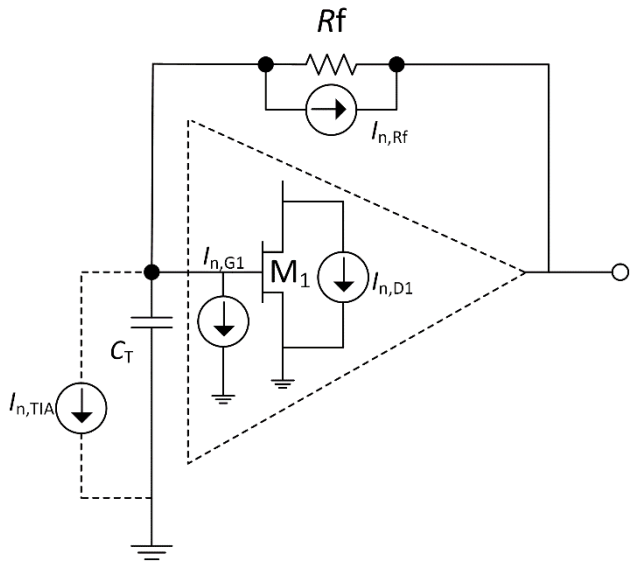

Fig. 7 Simplified noise model of the TIA

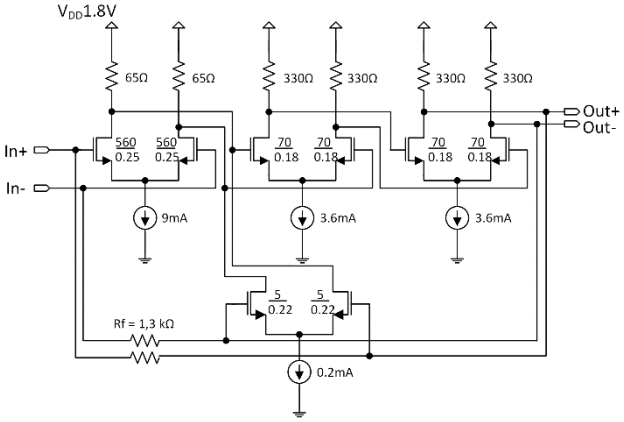

Fig. 8 Schematic of the TIA

3.1.2 Post-amplifier

The purpose of the post-amplifier is to amplify the output pulse of the preamplifier further to a suitable level for the timing comparators. The post-amplifier consists of three resistor loaded differential pair stages. The gain of the post-amplifier was set to ~ 10 and thus the effective transimpedance of the whole channel is ~ 26 kΩ. The bandwidth of the post-amplifier should not be too wide because it makes additional pole to the receiver system and is filtering the HF noise from the TIA and thus reducing the total noise. However, if two stages with equal band-widths are cascaded, then the overall small-signal bandwidth is narrower and thus the bandwidth of the post-amplifier was designed to be ~ 1.5 GHz (Fig. 9).

The circuit includes continuous-time offset cancellation which prevents the amplifier from being saturated by the offset due to device mismatch. In this way the heavily loading and area hungry AC coupling capacitors can be avoided. Fig. 10 shows the offset compensation realization where a trans-conductance element (Gm) is connected to the transconductance cell (M_4). M_3 has a constant bias voltage and the feedback path is incorporated with the input differential pair (M_1, M_2) of the post-amplifier. A transconductance element is basically a very slow operational amplifier with a diode connected load (Fig. 9). The voltage mismatch between input sensing lines of the Gm amplifier (offset) composes the voltage to the input of the M_4 differing from the constant VB_{const} at the M_3 input. The feedback path (M_3 and M_4) then creates the voltage difference to the input of the post-amplifier cancelling the offset. The corner frequency of resulting high-pass filter in the feedback loop needs to be low (offset is a DC behavior) and it is realized

with an external capacitor [25, 26]. However, while the unwanted offset caused by the device mismatch is cancelled, the offset voltage can also be controlled externally by forcing a desired voltage mismatch between the sensing lines (Gm input). It is realized by connecting an adjustable resistor (basically working as a current generator) together with the internal 5 kΩ ohm resistor to the input of the Gm circuit and it enables one to set the offset to a desired value for the comparators (see Fig. 10).

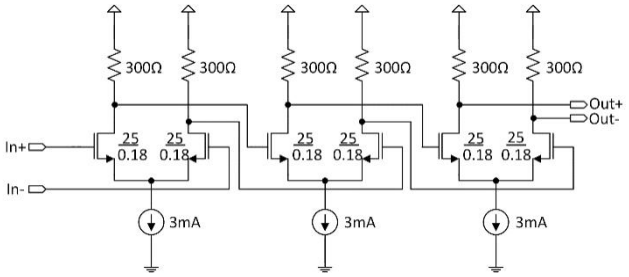

Fig. 9 Schematic of the post-amplifier

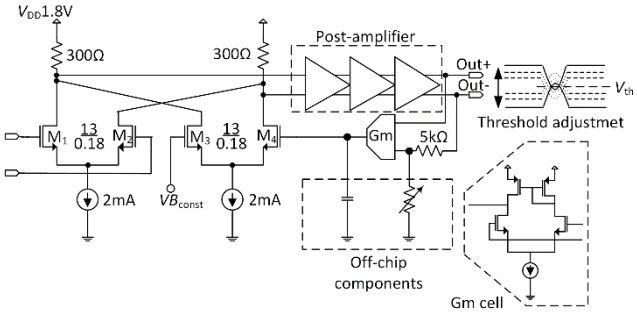

Fig. 10 Schematic of the offset compensation together with the threshold adjustment structure

3.1.3 Comparators and level shifting

The timing comparator used in this chip includes six identical amplifying stages and a latch (Fig. 11). The gain of one single stage was sized to be ~ 3, which is relatively low, but guarantees enough bandwidth for the stage. Several stages are needed in order to obtain enough gain for detecting a few millivolts' crossing of the comparator threshold. On the other hand the change of the delay of the comparator for low (slow slew rate) and high amplitude (fast slew rate) signals needs to be smaller than the jitter coming from the signal itself [14]. The latch further increases the speed and reduces the switching noise since the comparator changes the state only once after reset. The threshold for the comparator is set with the offset cancellation circuit so that the threshold is forced to the wanted value by external current as already described.

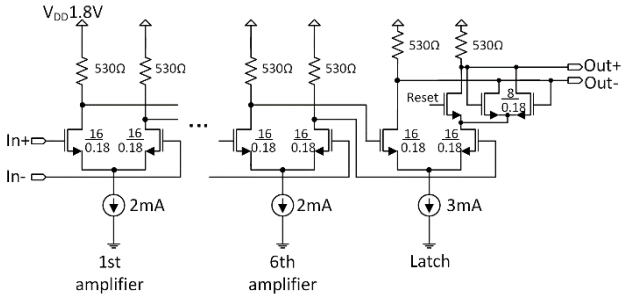

Fig. 11 Schematic of the comparator

The chip is intended to be used with a Time-to-Digital Converter (TDC) chip with 3.3 V supply voltage, and thus the receiver chip with 1.8 V output pads needs level shifting. To avoid the use of an external level shifter, a HV-CMOS technology is used. It allows 5 V transistors,

and an internal level shifter can be implemented. The schematic diagram of the level shifter is shown in Fig.12. The transistors are 5 V devices enabling to use of 3.3 V supply voltages and thus they give a 3.3 V output swing.

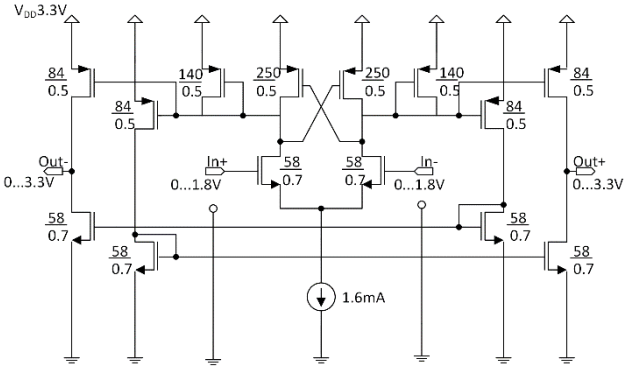

Fig. 12 Schematic of the level shifter

3.1.4 Analog output buffer

An analog output buffer was designed to drive the testing instrument outside the chip. To allow for a large output swing, differential buffers must employ wide transistors, thus exhibiting a high input capacitance. A "pre-driver" stage is therefore needed to drive an output stage with fast transitions [25]. Fig. 13 shows the schematic diagram of the output buffer consisting of a pre-driver stage and an open collector stage with external inductive peaking.

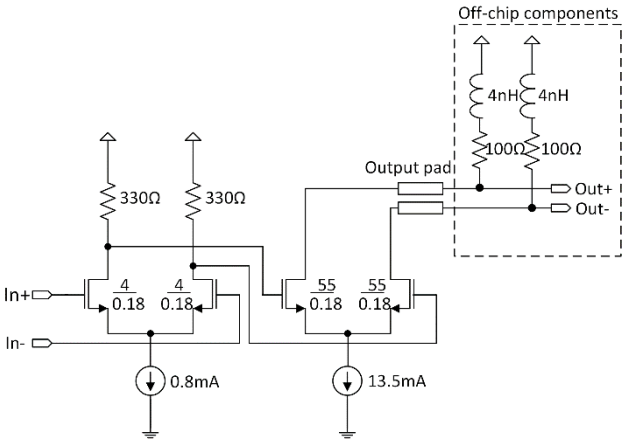

Fig. 13 Output buffer

4 MEASUREMENT RESULTS

The designed circuit was fabricated in a 0.18 HV-CMOS technology that allows the use of 5 V, 25 V, and 50 V as well as 1.8 V transistor devices. The receiver channel together with the timing discrimination was designed with 1.8 V supply voltage devices, and the CMOS level shifter together with the output pads for the STOP signals was using 5V transistors. A photograph of the receiver circuit is shown in Fig. 14. The total area of the chip is 2 mm^2 and power consumption of digital parts 45 mW, amplifier stages 79 mW, biasing and output buffer 57 mW and level shifter 20 mW (180 mW total).

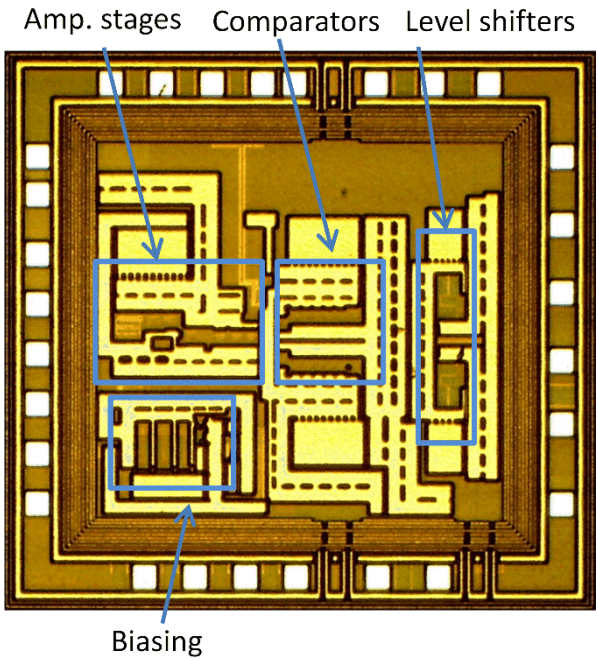

Fig. 14 A photograph of the receiver chip

Measurements were performed using the optical pulse (6 W/120 ps (FWHM)) from the laser transmitter presented earlier. The optical pulse was focused on a fiber and the neutral density (ND) filters was used to enable to attenuate the incoming pulse before it was focused on the APD (needed in the tests). The block diagram of the measurement system is presented in Fig. 15. The architecture of the TDC is presented in [30].

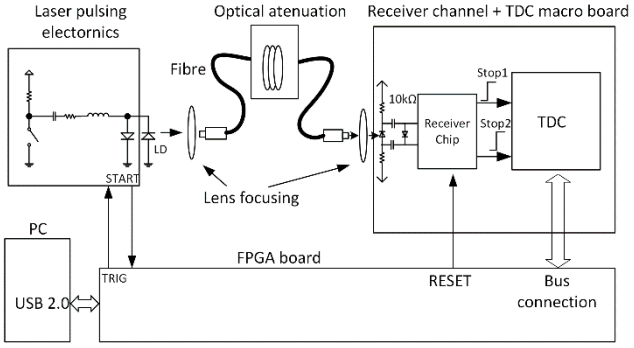

Fig. 15 Measurement setup

The bandwidth of the channel was measured with spectrum analyzer to be 635 MHz at the output of the output buffer. In simulations, the bandwidth from the output buffer was slightly smaller than the bandwidth of the channel itself and thus the total bandwidth of the channel can be estimated to be ~ 700 MHz with the estimated input total capacitance of 1.5 pF. Fig.16 shows the simulated and measured bandwidth. The transimpedance of the channel was measured by driving a differential current pulse from the signal generator to the input of the channel and probing the output voltage from the output buffer. It was measured to be 25.3 kΩ. Fig. 17 shows the noise voltage probed with the spectrum analyzer from the output buffer. The Y-axis shows the noise voltage, and the input referred noise current can be calculated by dividing the RMS noise of the TIA with its transimpedance (see equation (1)). It is ~ 340 nA from the output buffer. However, the narrower bandwidth and the attenuation of the output buffer need to be taken into account, and the total input referred noise current of the receiver was estimated to be approximately 450 nA. The first term of the noise equation (eq. (3)) represents the thermal noise coming directly from the R_f, and it can be calculated to be ~ 200 nA for 1.3 kΩ. As ~ 20 nA is coming from the thermal noise of the 10 kΩ bias resistors of the APD, roughly half of the noise is generated by the amplifier itself.

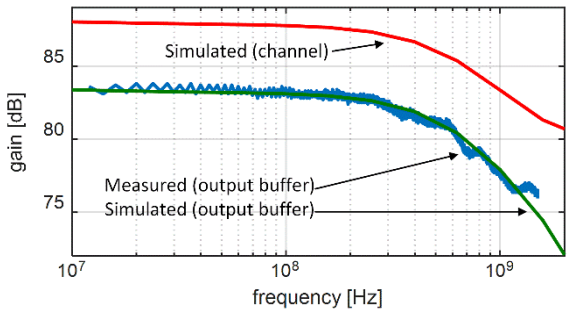

Fig. 16 Measured bandwidth from the receiver output buffer (blue) and simulated (green) and simulated bandwidth of the channel (red)

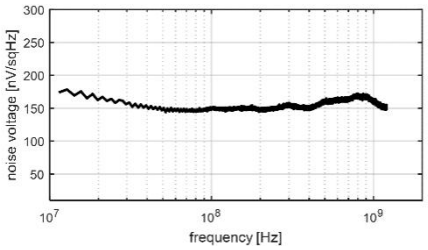

Fig. 17 Measured noise voltage from the output buffer

Fig 18 shows the shape of the laser pulse used in this work measured with a ~ 25 GHz optical probe. Fig. 19 shows the time domain pulse shapes probed from the analog output buffer of the receiver. There are three pulses in the figure where green illustrates the lowest that crosses the comparator threshold set to the level of SNR = 10 and blue is from a higher input but still within the linear range of the channel. The red response indicates a pulse saturating the channel. The dynamic range of the output buffer is 450 mV and for the channel itself ~ 900 mV, which means that the input signals from 4.5 µA to 40 µA (SNR = 10 to 80) can be observed without clipping.

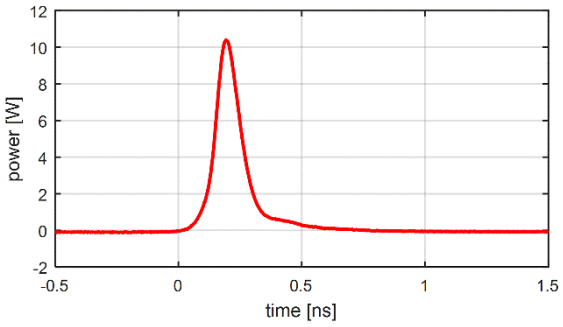

Fig. 18 Pulse shape of the laser pulse

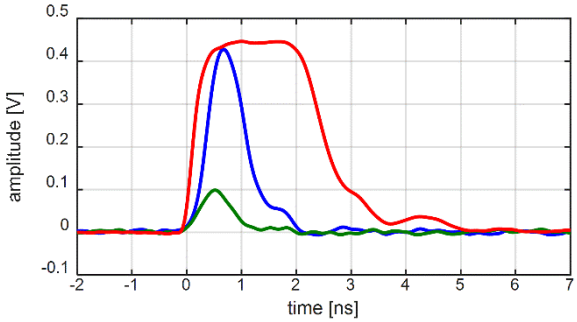

Fig. 19 Pulse shape probed from the output buffer

The timing walk error was measured by sweeping the input signal from 4.5 µA to 95 mA giving a dynamic range of 1:21,000 (Fig. 20). The minimum signal was chosen to be ten times higher than the input referred noise current (SNR 10) to avoid unwanted stops from the noise spikes. The threshold of the comparator was set to be at the level of SNR 6. It can be seen that the total walk error caused by the channel delay and the pulse geometry is 470 ps. Fig. 21 shows the measured jitter of the leading edge as a function of input amplitude. The maximum jitter with the minimum signal is 62 ps, lowering to 11 ps at higher signal amplitudes. The jitter of the start pulse coming from the pulsing device and the jitter of the TDC (~10 ps) are affecting the total jitter setting limit to ~ 10 ps. 11 ps corresponds 1.65 mm in distance, and 62 ps 9.3 mm when the time-of-flight method is used. Low jitter enables to achieve a very accurate single-shot precision when leading edge detection is used. The walk error can be compensated either by using the slew rate or pulse width measurement based method presented in [31] and [32], respectively or both methods [33]. Table 1 shows the performance summary of the proposed receiver chip in comparison with some recently published works. The use of sub-ns laser pulses in this work is a new feature and it obviously calls for the widest bandwidth. As a result, the intrinsic walk error is about four times smaller than in the other works. High speed of the laser pulse also improves the single-shot precision (discriminated from the leading edge of the pulse) with a factor of ~ 3 at SNR = 10. The jitter of the TDC is at the level of ~ 10 ps and is probably limiting the highest achievable precision.

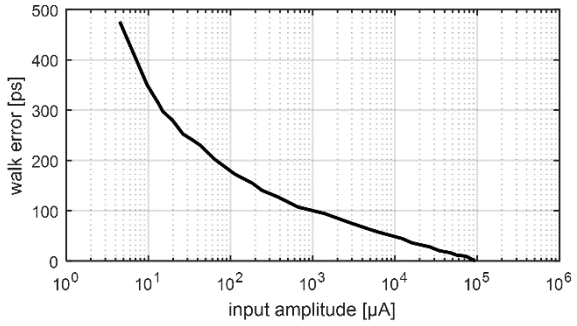

Fig. 20Walk error as a function of input amplitude

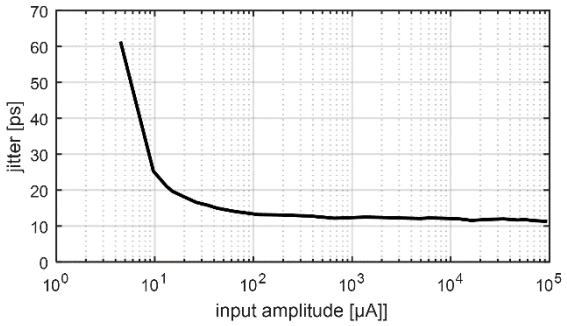

Fig. 21 Jitter of the leading edge of the pulse as a function of input amplitude

	This work	[34]	[35]	[36]	[37]
Technology	CMOS 0.18 µm	CMOS 0.13 µm	CMOS 0.13 µm	CMOS 0.35 µm	discrete
C_{IN}	1.5 pF	2 pF (C_{PD})	1.5 pF (C_{PD})	2.5 ~ 5 pF	NA
Pulse width	100 ps	1 ns	3 ns	5 ns	50 ns
Power consumption	180 mW (V_{dd} 1.8 V)	110 mW (V_{dd} 1.2 V)	45 mW (V_{dd} 1.2 V)	NA (V_{dd} 3.3 V)	NA
Band width	700 MHz	>500 MHz	300 MHz	140 MHz	6 MHz
Precision	9.3 mm @ SNR 10	NA	38 mm @ SNR 10	NA	29 mm @ SNR 7
Dynamic range	1:21,000	1:1,600 (linear)	1:10,000	1:12,000	1:80
Intrinsic walk error	0.47 ns	1.7 ns	2.2 ns	2.8 ns	NA
minimum jitter	11 ps	NA	NA	NA	NA

TABLE 1

5 CONCLUSIONS

A receiver channel for a pulsed TOF laser radar with low detection jitter and walk error is presented. The channel is intended to be used with a laser diode transmitter generating high power sub-ns pulses. The receiver is realized in a 0.18 µm HVCMOS technology. Leading edge detection of the timing pulse is used. The total walk error of the channel in the dynamic range of 1:21,000 is 470 ps and the jitter of the leading edge of the detected pulse is 62 ps at the SNR of ~ 6 lowering to ~ 10 ps at the higher signal amplitudes limited by the jitter of the time-to-digital converter chip.

The low jitter of the receiver could possibly be utilized e.g. for the measurement of tiny vibrations of distant objects. For example, by averaging the 1,000 single-shot measurements, the precision is at the level of < 0.3 ps, which corresponds to ~ 50 µm in distance measurement. The measurement time for this precision would be 1 ms at the pulsing rate of 1 MHz.

LIST OF REFERENCES

[1] Ruotsalainen, T., Palojärvi, P. & Kostamovaara, J. (1997). *A BiCMOS differential amplifier and timing discriminator for the receiver of a laser radar*. Analog Integrated Circuits and Signal Processing, 13, 341–352.

[2] Chen, Y., Meng, Z., Liu, J., & Jiang, H. (2011). High precision infrared pulse laser ranging for active vehicle anti-collision application. Electric Information and Control Engineering (ICEICE), 1404–1407.

[3] Lee, M., & Baeg, S.H. (2012*). Advanced compact 3D LIDAR using a high speed fiber coupled pulsed laser diode and a high accuracy timing discrimination readout circuit.* Proc of SPIE Laser Radar Technology and Applicatons XVII, 879, 8379Z.

[4] Cho, H. –S., Kim, C. –H., & Lee, S. –G. (2014). *A high-sensitivity and low-walk error LADAR receiver for military application*, IEEE Transactions on circuits and systems-I, 61(10), 3007–3015.

[5] Vainshtein, S., Yuferev V.S., Kostamovaara, J. (2002). *Properties of the Transient of avalanche transistor switching at extreme current densities.* IEEE Transactions on Electron Devices, 49(1), 142–149.

[6] Lanz, B., Ryvking, B., S., Avrutin, E., A. & Kostamovaara, J. (2013). *Performance improvement by a saturable absorber in gain-switched asymmetric-waveguide laser diodes*. Optics Express, 21(24), 29780–29791.

[7] Hallman L.W., Ryvikin B., Haring K., Ranta S., Leinonen T., & Kostamovaara J. (2010). *Asymmetric waveguide laser diode operated in gain switching mode with high-power optical pulse generation*. Electronics Letters, 46(1), 1–2.

[8] Hallman, L. W., Huikari, J., & Kostamovaara, J. (2014). A high-speed/power laser transmitter for single photon imaging applications. IEEE Sensors, 1157–1160.

[9] Ryvkin, B., S., Avrutin, E., A. & Kostamovaara, J. (2009). *Asymmetric-Waveguide Laser Diode for High-Power Optical Pulse Generation by Gain Switching*. Journal of Lightwave Technology, 27(12), 2125–2131.

[10] Lau, K. Y. (1988). *Gain switching of semiconductor injection lasers.* Applied physics letters, 52(4), 257–259.

[11] Bimberg, D., Ketterer, K., Bottcher, E. H. & Scoll, E. (1986*). Gain modulation of unbiased semiconductor lasers: ultrashort pulse generation*. International Journal of Electronics, 60(23), 23–45.

[12] Volpe, F., P., Gorfinkel, V., Sola, J. & Kompa, G. (1994). 140 W/40 ps single optical pulses for sensor application, Conference on Lasers and Electro-Optics, Anaheim, CA, USA, May 8 – 13, 1994.

[13] Vainshtein, S. & Kostamovaara, J. (1998). *Spectral filtering for time isolation of intensive picosecond optical pulses from a Q-switched laser diode*. Journal of Applied Physics, 84(4), 1843–1847.

[14] Van de Plassche, R. J. (1988). *An 8-bit 100-MHz Fully-Nyquist Analog-to-Digital Converter*. IEEE Journal of Solid State Circuits, 23(6), 1334–1344.

[15] Säckinger, E. (2005). *Broadband Circuits for Optical Fiber Communication.* Hoboken, NJ.

[16] Carcia del Pozo, J. M., Serdijn, W. A., Otin, A., & Celma., S. (2011). *2.5 Gb/s CMOS preamplifier for low-cost fiber-optics receivers*. Analog Integrated Circuits and Signal Processing, 66, 363–370.

[17] Han, S. M., Sun, G., Jiang, F., Yu, X-P., & Wu X.B. (2009). *Area-efficient CMOS transimpedance amplifier for optical receivers.* Analog Integrated Circuits and Signal Processing, 58, 67–70.

[18] Zheng, H., Ma, R. & Zhu, Z. (2017). *Design of linear dynamic range and high sensitivity matrix quadrant APDs ROIC for position sensitive detector application.* Microelectronics Journal, 63, 49–57.

[19] Ma, R., Liu, M., Zheng, H. & Zhu, Z. (2017). A 77-dB Dynamic Range Low-Power Variable-Gain Transimpedance Amplifier for Linear LADAR. IEEE Transactions on Circuits & Systems II Express Briefs, DOI:10.1109/TCII.2017.2684822.

[20] Abramowitz, M., & Stegyn, I.A. (1964). *Handbook of mathematical functions with formula, graphs, and mathematical tables*. Dover publications.

[21] McIntyre, B. J. (1970). *Comparison of photomultipliers and avalanche photodiodes for laser applications*. IEEE Transactions on Electron Devices. 17(4), 347–352.

[22] Wang, J. & Kostamovaara, J. (1994). *Radiometric analysis and simulation of signal power function in a short-range laser radar.* Applied optics, 33(18), 4069–4076.

[23] Hintikka M., & Kostamovaara J. (2015). Time domain characterization of avalanche photo detectors for sub-ns optical pulses, International Instrumentation and Measurement Technology Conference, pp. 2015–2019.

[24] Cherry, E., M. & Hooper, D., E. (1968). The Design of Wideband Transistor Feedback Amplifiers. Proc. IEE, 110, 375–398.

[25] Galal, S., & Razavi, B. (2003). *10-Gb/s limiting amplifier and laser/modulator driver in 0.18 um CMOS technology*. IEEE Journal of Solid-State Circuits, 38(12), 2138−2146.

[26] Huang, S-H., Chen, W-Z., Chang, Y-W., & Huang, Y-T. (2011). *A 10-Gb/s OEIC with Meshed Spatially-Modulated Photo Detector in 0.18-um CMOS Technology*. IEEE Journal of Solid State Circuits, 46(5), 1158−1169.

[27] Zheng, H., Ma, R. & Zhu, Z (2017). *A linear and wide dynamic range transimpedance amplifier with adaptive gain control technique.* Analog Integrated Circuits and Signal Processing, doi: 10.1007/s10470-016-0867-1.

[28] Abidi, A. A. (1987). *On the Noise Optimum of Gigahertz FET Transimpedance Amplifiers*. IEEE Journal of Solid State Circuits, SC-22(6), 1207−1209.

[29] ZhiQun, L., LiLi C., Wei L. & Li Z. (2012). *A 12x10 Gb/s fully integrated CMOS parallel optical receiver frong-end amplifier array*. Science China, 55(6), 1415–1428.

[30] Jansson J., Koskinen V., Mäntyniemi A., & Kostamovaara J. (2012*). A multi-channel high precision CMOS time-to-digital converter for laser scanner based perception systems*. IEEE Transactions on Instrumentation & Measurement, 61(9), 2581–2590.

[31] Kurtti, S., & Kostamovaara, J. (2009). *Pulse width time walk compensation method for pulsed time-of-fligh laser rangefinder*. Interantional Instrumentation and Measurement Technology Conference, Singapore, May 2009.

[32] Nissinen, J., & Kostamovaara, J. (2007). *An integrated laser radar receiver channel with wide dynamic range.* Electronics, Circuits and Systems 14th IEEE international Conference, pp. 10–13.

[33] Kurtti, S., Nissinen, J. & Kostamovaara, J. (20017). *A wide dynamic range CMOS laser radar receiver with a time-domain walk error compensation scheme*, IEEE Transactions on Circuits and Systems I, Regular Papers, 64(3), 550–561.

[34] Ngo, T.-H., Kim, C.-H., Kwon, Y. J., Ko J.S. Kim, D.-B. & Park H.-H. (2013). *Wideband receiver for a three-dimensional ranging LADAR system*. IEEE Transactions on Circuits and Systems I Reg. papers, 60(2), 448–456.

[35] Nissinen, J., Nissinen, I. & Kostamovaara, J. (2009). *Integrated receiver including both receiver channel and TDC for a pulsed-time-of-flight laser range finder with cm-level accuracy*. IEEE J. Solid-State Circuits, 44(5), 1486–1497.

[36] Cho, H.-S., Kim, C.-H. & Lee S.-G. (2014). *A high-sensitivity and low walk error LADAR receiver for military application.* IEEE Transactions on Circuits and Systems I, Reg. Papers, 61(10), 3007–3015.

[37] Xiao, J., Lopez, M., Hu, X., Xiao, J. & Yan, F. (2016). *A continuous wavelet transform-based modulus maxima approach for the walk error compensation of pulsed time-of-flight laser rangefinders.* International Journal for Light and Electron Optics, 127(4), 1980–1987.